Forest Change Detection Using Google Earth Engine: A Temporal Analysis of Shirani District

Shafi Ullah
shafi.ullah@buitms.edu.pk
Department of Computer Engineering, Balochistan University of Information Technology, Engineering & Management Sciences (BUITEMS), Quetta 87300, Pakistan

Niamat Ullah
niamatullahza@gmail.com
Spatial Decision Support System (SDSS)Lab, NCGSA, Balochistan University of Information Technology, Engineering & Management Sciences (BUITEMS), Quetta 87300, Pakistan

Ahsanullah Memon
ahsanmemon@muetkhp.edu.pk
Electrical Engineering Department Mehran Univerity SZAB Campus Khairpur, Pakistan

Shanila Azhar
shanila.azhar@buitms.edu.pk
Department of Computer Engineering, FICT, Balochistan University of Information Technology, Engineering & Management Sciences (BUITEMS), Quetta 87300, Pakistan

Bakhtiar Khan Kasi
bakhtiar.kasi@buitms.edu.pk
Department of Computer Engineering, Balochistan University of Information Technology, Engineering & Management Sciences (BUITEMS), Quetta 87300, Pakistan

Corresponding Author:* Shafi Ullah shafi.ullah@buitms.edu.pk

Received: 13-01-2025 **Revised:** 22-01-2025 **Accepted:** 11-02-2025 **Published:**01-03-2025

ABSTRACT

Forest fires are a common and devastating natural disaster that causes widespread damage to forest vegetation and poses significant threats to ecosystems. Detecting and monitoring forest fires are crucial for mitigating their impact on the environment and human communities. This research paper focuses on remotely monitoring the change detection in the Sherani Balochistan Pine Nut Forest, which experienced extensive fires, resulting in substantial damage to the Pine Nut crop. Being the world's largest Pine Nut crop, this event has significant implications for global nut crop production. The proposed solution utilizes remote sensing techniques to detect major changes in the Pine Nut Forest, with images depicting the Sherani forest fire collected from Landsat 9 satellite imagery. It involves actual fire detection, monitoring of damaged areas, and risk hazard analysis. The research employs temporal analysis, which examines the burned area at different time series to observe changes in the geographic area and potential loss of forest cover. Satellite imagery is obtained through the GEE for geospatial analysis, using Landsat data with a spatial resolution of 30 meters for improved comparison and collation of semi-centennial forest data. The approach involves the calculation of indices for the Pine Nut Forest using the NBR and dNBR. These indices help identify the extent of affected land and the severity of the burn. By utilizing this novel approach, the forest department can effectively detect changes in land and climate, enabling better decision-making based on the collected data. Overall, this research contributes to improved forest fire management and conservation efforts.

Keywords: *Google Earth Engine (GEE), Normalized Burn Ratio (NBR), Differenced Normalized Burn Ratio (dNBR)*

1. INTRODUCTION

A profound natural geo-hazard, forest fires hold the potential to become uncontrollable if timely action is not taken. These fires exhibit a remarkable capacity for rapid dissemination, swiftly engulfing vast expanses of terrain and inflicting extensive damage upon ecosystems. The ensuing consequences are characterized by significant losses in vegetation, leading to irreparable devastation of crops and trees endemic to the affected forests (Han et al., 2017). The forest fire engenders a significant extent of destruction across a wide coverage area, extending beyond mere vegetation damage. Its impact reverberates beyond the ecological realm, affecting nearby communities, rescue teams dedicated to forest preservation, and a myriad of animals residing within the ecosystem. The confluence of dense smoke and prolonged fire duration leads to the demise of avian species. Moreover, the sustained blaze for several days has multifaceted repercussions, including implications for neighboring residences and inhabitants near the forest (Petkovic et al., 2020). The annual forest fires reach a high percentage which disturbs most of the earth's forest area. Forest fires occur in most places and mostly happen annually (Schroeder et al., 2014). It is the most common type of natural disaster happening in some specific places every year.

Remote Sensing's versatile, scalable, and adaptable nature has ushered advancements across diverse disciplines. It stands as a pivotal factor driving progress in various domains (Shimabukuro & Smith, 1991). Remote sensing enables comprehensive observations across multiple sectors, including risk management, forest monitoring, and land/cover area surveillance, through the analysis of satellite images (Arai et al., 2019). Remote sensing encompasses three primary modalities: ground-level data collection from tall towers, aerial data acquisition via UAVs (Unmanned Aerial Vehicles) and helicopters, and satellite imagery sourced from satellites such as MODIS, Sentinel, and Landsat. This research focuses on utilizing Landsat imagery to gather information about the BalochistanShirani Pine-nut Forest.

Utilizing Google Earth Engine (GEE) tools, satellite imagery becomes a potent resource for monitoring diverse regions. Specifically, this research employs GEE to oversee the Koh-e-Sulaiman region's Baluchistan Shirani area, which boasts the world's largest Pine-Nut Forest. At the outset of 2022, this expanse experienced a devastating fire that endured for nearly two weeks, resulting in substantial forest destruction. This forest is currently susceptible to extensive fires, inflicting widespread damage upon the Pine-nut Forest and compromising nut crop yields. This incurs a profound impact on global nut crop production, signifying a substantial loss in Pine Nut resources on a global scale (Szpakowski& Jensen, 2019). In 2022, the forest fires in the Pine Nut Shirani region resulted in a substantial 40% damage to the global Pine nut crop. The primary impact of these fires is inflicted upon both the forest vegetation and the crops it sustains. Employing the Landsat approach facilitated by the Google Earth Engine (GEE) tool, satellite images will be harnessed for fire analysis. GEE's geospatial analysis of satellite imagery aids in detecting areas of loss, as it effectively maps the burned regions. The integration of Landsat data enables efficient detection of the burned areas, contributing to accurate assessment (Gargiulo et al., 2021).

Landsat provides satellite images of years which help in the collection of datasets and more data provide a better comparison of the degradation of the forest (Babu&Vanama, 2020). Landsat offers superior resolution, utilizing the Operational Land Imager (OLI) data to deliver optimal satellite imagery at a resolution of 30 meters. When juxtaposed with alternatives such as MODIS and VIIRS, Landsat consistently yields more favorable results, particularly in forest fire detection, owing to its finer resolution and enhanced comparative performance (Suresh &Vanama, 2018; Bin et al., 2013). Landsat, synergistically paired with the Google Earth Engine (GEE), furnishes Shirani Baluchistan's satellite images. Leveraging this imagery, pre-fire and post-fire data can be analyzed to discern

transformations within the Pine-Nut Forest. This comparative analysis effectively identifies damaged regions, establishing a threshold for change detection. It yields essential insights into the extent of fire-induced expansion and destruction within the Shiraniforest area.

Initiating in Baluchistan, the fire's uncontrolled progression reached parts of the Khyber Pakhtunkhwa province, exacerbating the situation. Employing the temporal data analysis facilitated by the Landsat approach, calculated indices enable the detection of changes within the Pine Forest. Furthermore, these indices facilitate the straightforward identification of burn severity, providing a comprehensive understanding of the fire's impact (Wang et al., 2010). Utilizing appropriate indices, particularly through the Landsat approach, change detection within the Pine Forest is facilitated. The application of indices such as the Normalized Burn Ratio (NBR) and Differenced Normalized Burn Ratio (dNBR) streamlines the identification of burn severity and changes within the pine forest. This innovative method empowers the forest department to effectively discern shifts in both land and climate conditions, capitalizing on the amassed data to draw informed conclusions. The inherent capability of our approach extends to the straightforward identification of diverse changes, encompassing alterations in land cover and climate dynamics.

2. RELATED WORK

Forest fires, as natural geo-hazards, epitomize uncontrolled infernos that ravage without restraint, leaving extensive devastation in their wake. These uncontained fires wreak havoc, exacting colossal losses upon the impacted regions. The rampant nature of these fires precipitates not only substantial forest damage but also impinges on crops, local inhabitants, and their dwellings. This paper delves into methods to mitigate and forestall forest fires, underscoring the critical need for proactive measures to avert further catastrophe (Petkovic et al., 2020). Remote sensing plays a pivotal role across various domains due to its ability to provide precise and comprehensive observations from a distance. Its significance is particularly pronounced in managing diverse fields. The application of remote sensing encompasses a range of critical functions, including risk mitigation, forest surveillance utilizing remote sensor methodologies, and continuous monitoring of both forested and terrestrial regions. This research focuses on the utilization of Google Earth Engine (GEE) to facilitate forest monitoring. Employing the Sentinel-1 approach, this study aims to amass pertinent data essential for achieving these objectives (Gargiulo et al., 2021). This study focuses on analyzing a five-year dataset spanning from 2015 to 2020. The primary objective is to perform a comparative analysis of yearly data to detect changes, particularly concentrating on areas affected by fire-related incidents. By utilizing time series data, the research aims to visually depict alterations in the Pine Forest, showcasing both its forested expanse and the extent of degradation caused by fire-induced damage. The investigation primarily hinges on temporal data analysis to meticulously assess the outcomes of the comparative monitoring efforts.

The research adopts a temporal analysis approach to facilitate a comprehensive data comparison. This endeavor involves employing satellite imagery from both Sentinel-2 and Landsat-8 platforms within the Google Earth Engine (GEE) framework. The primary objective revolves around mapping the fire-affected regions across Australia and subsequently conducting a meticulous comparative assessment between the data derived from Sentinel-2 and Landsat-8. A noteworthy finding emerges from the comparison: the satellite images acquired from Sentinel-2 outshine those from Landsat-8 in terms of quality. This superiority is attributed to Sentinel-2's finer resolution, which significantly enhances the clarity of the imagery. Through the integration of Sentinel-2 imagery within the GEE platform, a more distinct depiction of the burned areas is achieved, enabling a more accurate identification of the fire-ravaged regions (Babu&Vanama, 2020).

The grasslands of Africa span a vast expanse and hold immense significance as a primary source of sustenance and habitat for various animal species. Preserving the grasslands, particularly in South

Africa, takes on heightened importance. Notably, the grassy regions in elevated or steep terrains are particularly vulnerable to transformation due to significant environmental shifts. These alterations could stem from climate variations, geological hazards, or even forest fires. Safeguarding these areas assumes paramount importance.

This study adopts a remote sensing methodology, employing both the Landsat-8 and Sentinel-2 platforms, to address these concerns. The objective is to compare the efficacy of these techniques in assessing the grasslands before and after fire incidents, consequently facilitating change detection analysis. Through this comparative approach, the research aims to glean insights into the effectiveness of each technique in capturing the alterations wrought by such events. The outcomes reveal that both the Landsat-8 and Sentinel-2 approaches yield robust results in identifying and delineating fire-affected areas. These techniques play a pivotal role in accurately pinpointing the burned regions, providing invaluable information to inform conservation efforts and management strategies (Semela et al., 2020).

3. METHODS AND MATERIALS

3.1 Study area

Sherani District spans an area of 4,310 square kilometers(PBS, 2024). It encompasses 1 Tehsil and 7 Union Councils. The focal study area of this research is SheraniBalochistan, situated at a latitude of 31°17’14 North and longitude of 70°2’28 East within the province of Balochistan. Sharing its eastern borders with South Waziristan, the district is positioned to the northeast of Quetta City, the provincial capital of Balochistan. Musakhail lies to the south, with Zhob District bordering the west. The district is characterized by its mountainous terrain within the Sulaiman Range with an elevation ranging from 678 to 3,356 meters.Geographically, Sherani lies approximately 325 km northeast of Quetta, the provincial capital of Balochistan. The total population of the district is 191,687 with an average household size of 5.31 and a population density of 44.47 people/km^2 (PBS, 2024). The total forest area within Sherani district spans 6,277 hectares.Zhob attained district status in 2006, followed by the subsequent division of Sherani from Zhob. The name derives from the Sheranitribe, a prominent local community in northeasternBalochistan. Shin Bazai stands as a notable town within the vicinity, while the district headquarters is situated in” StanoRaaghah” town. The district’s topography predominantly comprises towering mountains adorned with valuable” Chalghoza” trees, a source of both income and local pride. The local economy primarily relies on agriculture and livestock.

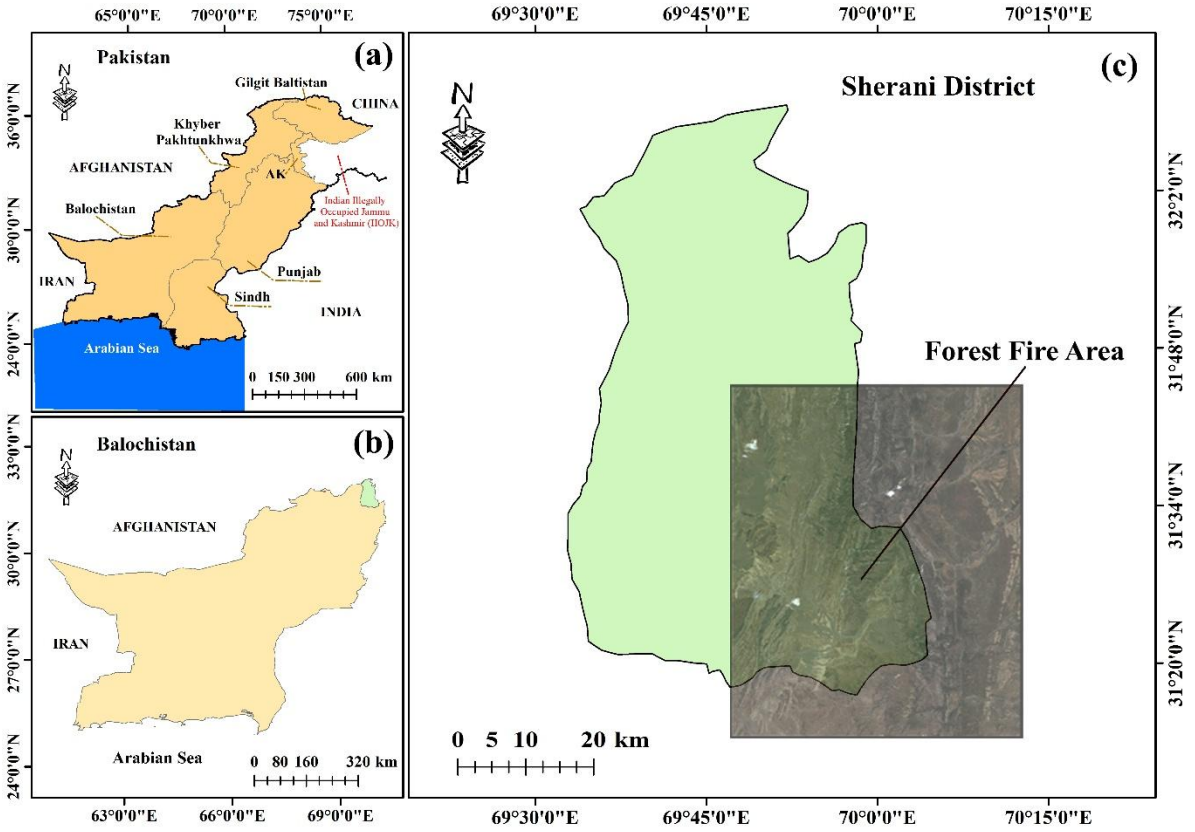

Figure 1. The geographic extent of Pakistan (a), Balochistan (b), and Sherani District (c).

3.2 Methods

In this segment, we provide an overview of Landsat and its application to the specified target site for our proposed topic using Google Earth Engine (GEE) tools (Izquierdo-Verdiguier et al., 2021). The detailed methodological workflow of the present study is depicted in Figure 2.

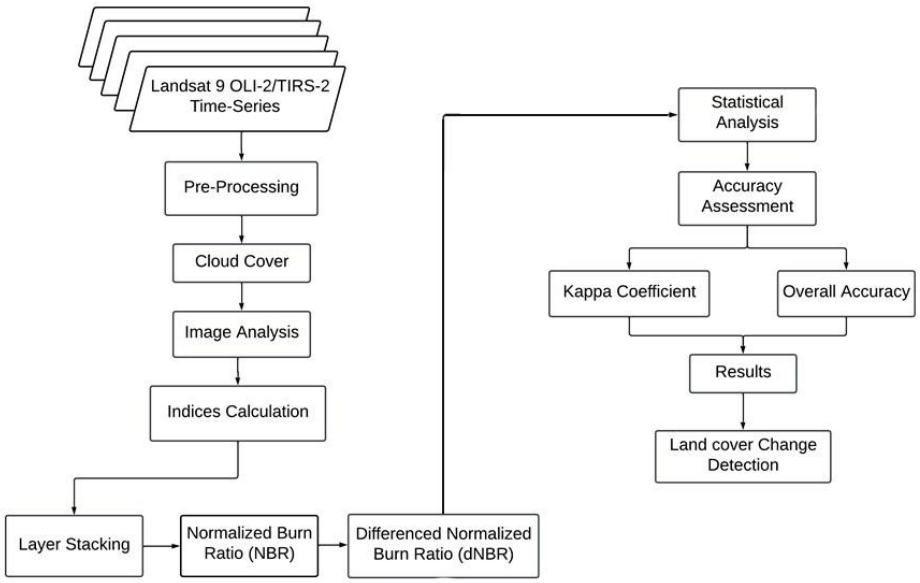

Figure 2. The detailed methodological workflow of the present study.

3.2.1 Landsat Overview

Landsat initially launched on July 23, 1972, has consistently provided aerial satellite images, accumulating data over nearly four decades. This uninterrupted Landsat dataset equips land managers and policymakers with vital information for informed decisions regarding natural resources and the environment, capturing space-based photographs of Earth's land surface. By 2022, nine Landsat satellites had been launched, marking their significance in remote sensing (Young et al., 2017). These remote sensing platforms amass extensive collections of satellite imagery, including visual and climate data, and were chosen for this thesis due to the unique 20-year dataset available, allowing for species distribution estimation and the identification of natural and human-induced changes on a larger scale. The diverse spectral bands of Landsat satellites find applications spanning ecology to geopolitics, with their continuous time series extending from 1972 to the present and a promising future with Landsat-9 (Banskota et al., 2014). This research section employed data from Landsat 9 to facilitate comprehensive analysis.

3.2.2. Landsat Data

The Landsat 9 satellite was utilized to collect images for the study area in 2022, providing a single-year dataset with images taken at a 30-meter resolution. Landsat 8 data accessibility extends from October 2021 to the present (Hair et al., 2018). To access the Landsat 8 dataset, a snippet of the Landsat 8 Earth Engine code must be incorporated into the JavaScript coding. Each Landsat dataset snippet is unique and specific to the satellite used. Landsat 9 features multiple bands, including SR B4 (RED), SR B3 (GREEN), and SR B2 (BLUE). Additionally, SR 10 is designated for surface temperature analysis

3.3 Pre-Processing

In the Pre-processing section, we delve into the initial stages of refining data. This segment comprehensively addresses the two pivotal elements: Cloud Cover and Striped Images.

3.3.1 Cloud Cover

In Landsat imagery, it is crucial to establish a specific threshold for Cloud Cover, ensuring it remains below a predetermined value. This is imperative to guarantee the accurate processing of the acquired images. In the designated study area, the utilization of Landsat satellite imagery is a pivotal step. Once the imagery undergoes initial filtration, it is imperative that the images subsequently undergo a Cloud Cover assessment. In this study area, the acceptable Cloud Cover limit is set at 15%. Exceeding this threshold leads to compromised image processing accuracy, resulting in distorted outcomes.

3.3.2 Striped Images

During the pre-processing phase of the study area, the Landsat 7 satellite images exhibit a striped pattern, stemming from a malfunction in Landsat 7's Scan Line Corrector on May 31, 2003. Through the implementation of various lines of code, these stripes can be effectively rectified, restoring the images to their original state. This challenge represents the primary limitation of Landsat 7 imagery. All images captured by Landsat 7 between 2003 and 2013 possess this striped appearance, which can be remedied by applying a specific corrective code, resulting in the restoration of the original image (El Fellah et al., 2016). Once this restoration is achieved, further processing can be conducted on the unblemished image. Notably, some data from the 2005 timeframe might still exhibit striped patterns and gaps due to the Scanner Row Prediction Anomaly associated with Landsat 7.

3.4 Indices

Spectral indices are essential for reducing brightness distortions like shadows and clouds while highlighting subtle spectral variations. They rely on the difference between two bands, averaged by their sum. These indices use a mathematical equation with 'n' integers, corresponding to spectral bands, to determine the index value for each pixel. In this study, the Normalized Burn Ratio (NBR) and Differenced Normalized Burn Ratio (dNBR) are used. NBR assesses burn area, while dNBR gauges severity. Using Landsat 9's 30-meter resolution imagery, captured pre- and post-fire, and Google Earth Engine, NBR values are compared for change detection in the Sherani district. This offers insights into fire impact on vegetation health and severity. In this study area, two different indices are applied to the forest fire in the Sherani district. The indices are as below:

3.4.1 Normalized Burn Ratio (NBR)

The Normalized Burn Ratio (NBR) pinpoints fire-affected areas and assesses burn severity. In the Sherani study, NBR reveals the burned land's extent and severity. Landsat 9 pro- vides relevant imagery, captured between May 8 and May 24, 2022. Leveraging Google Earth Engine (GEE), images are filtered and subjected to pre- and post-fire dates. NBR formula, applied when both dates are input, compares images for change detection. This process highlights burn-induced alterations. Filtered imagery is processed using the NBR formula for visualizing changes. The Normalized Burn Ratio (NBR) is calculated using the equation (1):

$$NBR = \frac{NIR-SWIR}{NIR+SWIR} \qquad (1)$$

The Normalized Burn Ratio (NBR) formula is calculated as (SR B5 - SR B7) / (SR B5 + SR B7), where SR B5 represents the Near Infrared band (NIR) and SR B7 represents the Short- wave Infrared band (SWIR). These band assignments vary among Landsat satellites. In later versions like Landsat 8 and 9, SR B5 is designated as Near Infrared (NIR), and SR B7 is designated as Short-wave Infrared (SWIR). This formula effectively captures spectral distinctions for accurate burn area assessment (Celik, 2018).

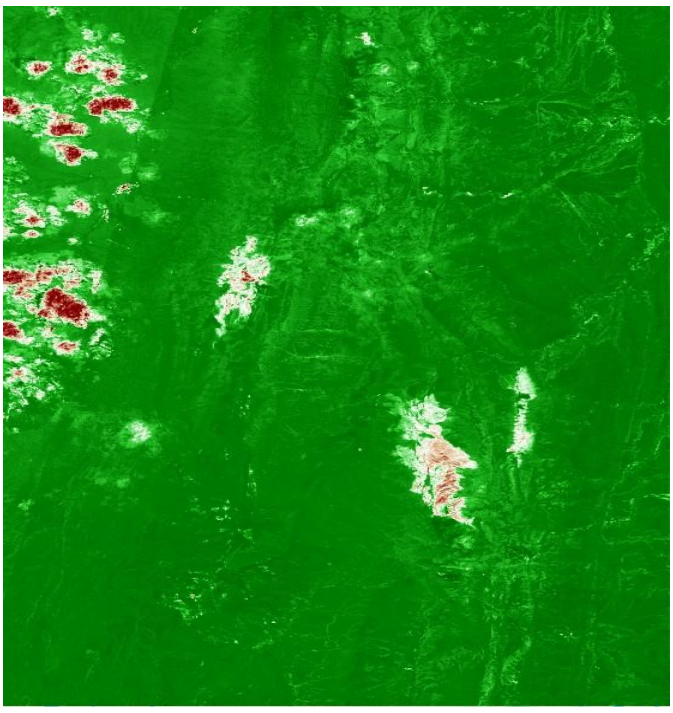

Figure 3. Detecting Changes with Normalized Burn Ratio (NBR)

3.4.2 Differenced Normalized Burn Ratio (dNBR)

The Differenced Normalized Burn Ratio (dNBR) is utilized to identify fire-affected areas and quantify burn severity. For assessing the extensive impact of burns, methods like dNBR are highly effective. In the study of the Sherani district, dNBR is applied to visualize burned regions and assess the severity of the burns. Landsat 9 satellite imagery acquired between May 8 and May 24, 2022, through Google Earth Engine (GEE), supports this analysis.

In this process, NBR values obtained from both Pre-fire and Post-Fire dates are subjected to filtration using the dNBR formula. This calculation indicates the severity of the burned land. The processed imagery, post dNBR formula, serves to visualize changes in the affected area (Miller and Thode, 2007). The formula for dNBR is as follows (2):

$$dNBR = NBR_{PreFire} - NBR_{PostFire} \quad (2)$$

The Differenced Normalized Burn Ratio (dNBR) is derived by subtracting the pre-fire Normalized Burn Ratio (NBR) from the post-fire NBR. This mathematical process yields the desired outcomes. Our computation of dNBR is achieved by analyzing the disparity between initial NBR imagery. We sought to evaluate NBR's effectiveness by employing this method-subtracting pre-fire from post-fire imagery. Remarkably, dNBR accentuates changes between NBR images, effectively highlighting fire presence. The computation involves filtering NBR images based on specific dNBR ranges. Noteworthy dNBR ranges include:

The initial two severity categories pertain to areas where fire-induced productivity increase is observed, specifically in grassy regions marked by strongly negative dNBR values, indicating elevated post-fire productivity (Figure 4). The bulk of non-burnt pixels is situated around the zero mark on the chart. The subsequent four levels encompass more extensively burned regions with notably positive dNBR values, often indicating recent burn activity.

S.no	Severity Level	Map Legend	dNBR Range
1	Enhanced regrowth, high		–0.5 to –0.251
2	Enhanced regrowth, low		–0.25 to –0.101
3	Non-burnt		–0.1 to 0.099
4	Low severity		0.1 to 0.269
5	Moderate-low severity		0.27 to 0.439
6	Moderate-high severity		0.44 to 0.659
7	High severity		0.66 to 1.3

Figure 4. Differenced Normalized Burn Ratio (dNBR) Spectrum with Severity Levels and Map Legend

3.4.3 dNBR Change Detection Analysis

The process involves segmenting the Pre-fire NBR from the Post-fire NBR, each traversing specific ranges that correspond to distinct colors. These colors signify the intensity of burn within specific areas as detected by dNBR's change analysis. The ranges are numerically defined within the code, ensuring precision across the entire study area. Change detection hinges on pixel-by-pixel comparison between Post-fire and Pre-fire pixels, carried out through 7 ranges, each associated with a unique color to visually represent the extent of change. This method is applied to the Sherani District, exemplifying change detection within a well-defined range of values. The specifics of Sherani's Change Detection are outlined below in Figure 5.

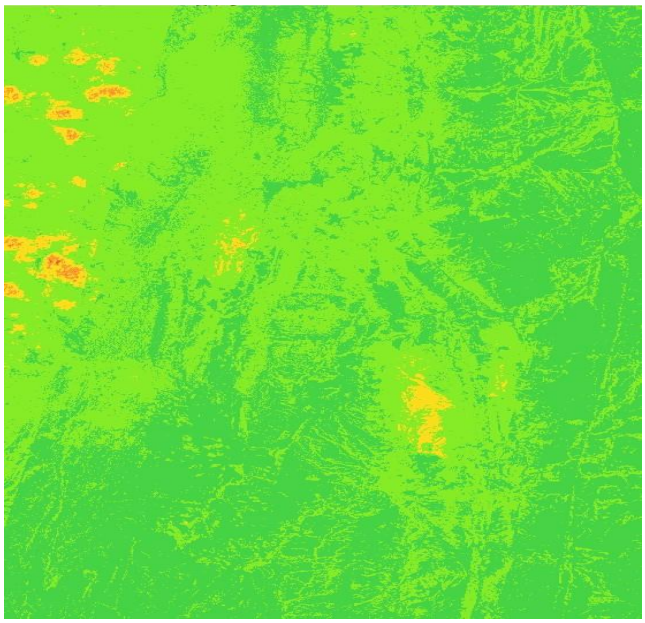

Figure 5.dNBR Change Detection Mapping Through dNBR Ranges

3.4.4 Change Detection Analysis

The process involves evaluating changes across various dNBR ranges. Every pixel is juxtaposed with the pre-fire state, generating a pixel-based visualization of the outcome. This approach yields results depicting pixel classes, corresponding hectares, and the total fire-affected area in hectares. The initial" Enhanced Regrowth" category indicates post-fire regrowth levels: high, low, or unburned, providing insights into the ecological response after the fire event. Subsequently, the last four categories present actual fire-related outcomes, capturing the severity and extent of fire impact.

The study area table, a pivotal component of this assessment, provides a comprehensive overview of the recorded data. It highlights the distribution of pixels across these distinct categories, enabling a quantitative understanding of the changes observed due to the forest fire. This detailed presentation facilitates both qualitative interpretation and quantitative analysis, fostering a deeper comprehension of the ecological dynamics in the aftermath of the fire event. The study area table is presented in Figure 6.

S.no	Classes	Pixels	Hectares	% of Total Area
1	Enhanced Regrowth, High	260	23.4	0.01
2	Enhanced Regrowth, Low	5497	494.73	5497
3	Unburned	49222	4429.98	1.98
4	Low Severity	1218925	109703.25	48.96
5	Moderate-low Severity	1212311	109107.99	48.69
6	Moderate-high Severity	3451	310.59	0.14
7	High Severity	03	0.27	0

Figure 6. Table Showing Results of Change Detection

3.4.5 Time Series Analysis

The scatter chart displays the Normalized Burn Ratio (NBR) values across different dates in May, coinciding with instances of fire occurrence. The chart effectively delineates the specified dates and is enhanced with a trendline that accentuates the Change Detection pattern. The chart is presented below:

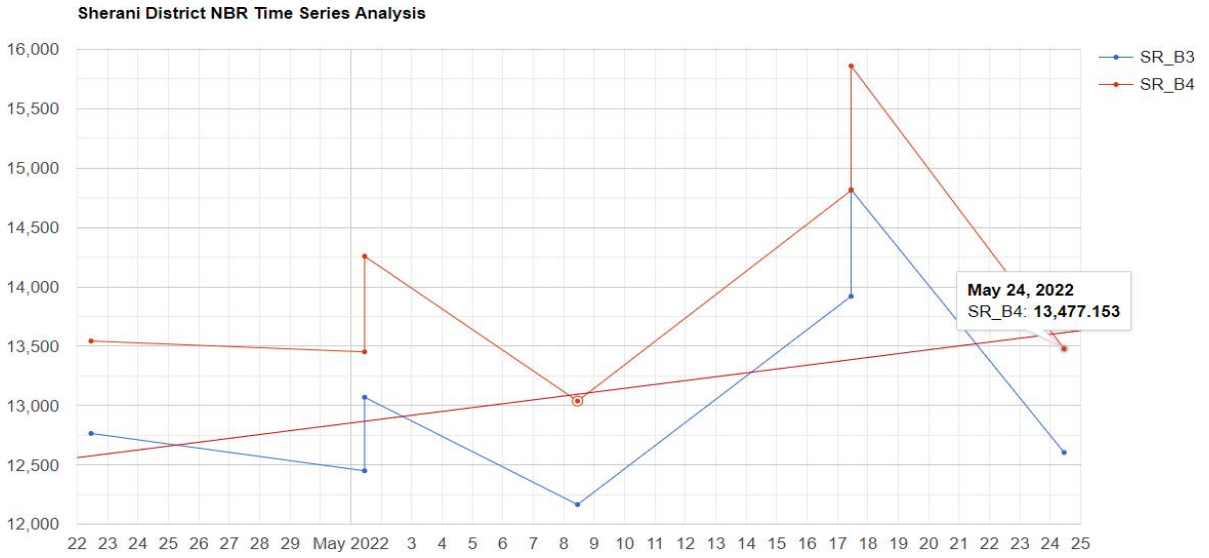

Figure 7.NBR-Time Series Analysis Depicting Forest Fire and Change Detection Trend

3.5 Accuracy

This results section presents both the overall accuracy and the Kappa Coefficient Analysis, providing a comprehensive assessment of the accuracy in change detection.

3.5.1 Overall Accuracy

Total accuracy serves as an indicator of how accurately the reference site is represented on the map. Typically presented as a percentage, overall accuracy attains 100% when a site is flawlessly classified. While offering foundational accuracy insights, overall accuracy remains the most straightforward to calculate and interpret. The formula for calculating overall accuracy is as follows (3):

$$\text{OverallAccuracy} = \frac{TP+TN}{P+N} (3)$$

The assessment of overall accuracy for the study area imagery is accomplished using the Overall Accuracy formula. By subjecting the classification to the overall accuracy calculation, we obtain the outcome for the study area, as presented below:

$$\text{Overall Accuracy} = 89.4$$

The result of the overall accuracy is 89.4 of the classification of the study area. Overall accuracy statistics are commonly used as a standard metric for the accuracy evaluation of categorized imagery.

3.5.2 Kappa Coefficient Analysis

To assess imagery accuracy, the Kappa coefficient is a widely adopted metric worldwide. It serves as a tool for evaluating image classification. Despite some criticisms, Cohen's Kappa statistic is commonly employed as a standard measure to evaluate the accuracy of categorized imagery (Pontius Jr &Millones, 2011; Stein et al., 2005). The error matrix approach, benefiting from the clear view of ground areas due to the burned forest canopy, enables more precise identification of high-burn fire

risk zones compared to low-burn areas. Incorporating dNBR alongside multispectral data enhances accuracy in fire risk determination (Walz et al., 2007; Epting et al., 2005).

Earlier studies achieved an overall accuracy of 85%, using either pixel-based or polygon-based methodologies for accuracy assessment. Our pixel-based technique yields a total accuracy of 89.4%, indicating a substantial level of accuracy for classification (Ye et al., 2018; Jensen et al., 1996). However, it's important to note that Cohen's Kappa statistics have limitations in accuracy measurement due to unpredictability, quantity conflict, and allocation disagreement (Pontius Jr &Millones, 2011).

The formula for Kappa coefficient analysis is (4):

$$\text{Kappa Coefficient} = \frac{P_0 - P_e}{1 + P_e} \quad (4)$$

Kappa Coefficient = 0.82

The result of the Kappa Coefficient is 0.82 for the classification of the study area. Kappa statistics are commonly used as a standard metric for the accuracy evaluation of categorized imagery.

3.5.3 Threshold

In this section, the threshold analysis examines pertinent indices and relies on their outcomes. If a value surpasses 0.66, the threshold generates a 'Yes' response, indicating discernible changes attributed to the forest fire. This visualization illustrates alterations in land cover and underscores the burn severity rate as well as change detection. Moreover, climate change detection illuminates forest and land soil transformations resulting from climatic shifts. Conversely, a 'No' outcome indicates that the indices discern no alterations between the pre-fire and post-fire conditions (Henry et al., 2017).

TABLE 1COHEN'S KAPPA AGREEMENT CATEGORIES

Valueofk	StrengthofAgreement
<0.20	Poor
0.21-0.40	Fair
0.41-0.60	Moderate
0.61-0.80	Good
>0.80	VeryGood

3.5.4 AccuracyDiscussion

Theachievedoverallaccuracyof89.4%intheclassificationof the study area is promising, indicating a strong agreementbetween the classified imagery and the reference data. Thishigh accuracy level suggests that the applied change detectionmethodology effectively captures the burn severity and land cover changes caused by forest fires. It is essential to consider the trade-offs between false positives and false negatives when interpreting the overall accuracy value. Furthermore, the Kappa coefficient analysis provides an additional layer of accuracy assessment by accounting for the agreement due to chance, enhancing the robustness of our accuracy evaluation (Gholinejad&Khesali, 2021).

4. CONCLUSION

In conclusion, this study underscores the effectiveness of remote sensing, particularly multispectral data, in identifying fire risk zones post-wildfires or human-induced fires. It highlights the importance of key indicators, including burnt trees and ground material abundance, in assessing surface burn severity through unmixing analysis. Landsat data, especially the dNBR index, was used to evaluate post-fire changes (Laneve et al., 2016). This research opens exciting possibilities for future applications using Google Earth Engine (GEE) technology, particularly for large-scale fire monitoring with Landsat data. Landsat time-series data prove invaluable for both visual and numerical change detection. The primary outcome of this study is the identification of fire hazards, fire danger detection, and damaged area mapping in the Sherani district. By employing indices like Normalized Burn Ratio (NBR) and Differenced Normalized Burn Ratio (dNBR), we successfully demonstrate change detection. This research contributes to enhanced forest fire management and conservation. It equips us to better respond to and mitigate the impact of forest fires, not only in the Sherani district but also in broader applications. The methodologies and tools introduced have the potential to bolster fire risk assessment and prevention strategies.

REFERENCES

1. Han, X., Zhong, Y., & Zhang, L. (2017). Spatial-spectral unsupervised convolutional sparse auto-encoder classifier for hyperspectral imagery. Photogrammetric Engineering & Remote Sensing, 83(3), 195-206.
2. Petkovic, M., Garvanov, I., Knezevic, D., &Aleksic, S. (2020). Optimization of geographic information systems for forest fire risk assessment. 21st International Symposium on Electrical Apparatus & Technologies (SIELA), 1-4. IEEE.
3. Schroeder, W., Oliva, P., Giglio, L., &Csiszar, I. A. (2014). The new VIIRS 375 m active fire detection data product: Algorithm description and initial assessment. Remote Sensing of Environment, 143, 85-96.
4. Shimabukuro, Y. E., & Smith, J. A. (1991). The least-squares mixing models to generate fraction images derived from remote sensing multispectral data. IEEE Transactions on Geoscience and Remote Sensing, 29(1), 16-20.
5. Arai, E., Shimabukuro, Y. E., Dutra, A. C., & Duarte, V. (2019). Detection and analysis of forest degradation by fire using Landsat/OLI images in Google Earth Engine. In IGARSS 2019 IEEE International Geoscience and Remote Sensing Symposium, 1649-1652. IEEE.
6. Szpakowski, D. M., & Jensen, J. L. (2019). A review of the applications of remote sensing in fire ecology. Remote Sensing, 11(22), 2638.
7. Gargiulo, M., Iodice, A., Riccio, D., &Ruello, G. (2021). Sentinel-1 time-series analysis for fires monitoring using Google Earth Engine tools. 6th International Forum on Research and Technology for Society and Industry (RTSI), 232-236. IEEE.
8. Babu, K. S., &Vanama, V. (2020). Burn area mapping in Google Earth Engine (GEE) cloud platform: 2019 forest fires in eastern Australia. International Conference on Smart Innovations in Design, Environment, Management, Planning and Computing (ICSIDEMPC), 109-112. IEEE.
9. Suresh, B. K., &Vanama, V. S. K. (2018). Fire detection in a varying topography using Landsat-8 for Nainital region, India. 3rd International Conference for Convergence in Technology (I2CT), 1-4. IEEE.
10. Bin, W., Jian, Y., Zhongming, Z., Yu, M., Anzhi, Y., Jingbo, C., Dongxu, H., Xingchun, L., &Shunxi, L. (2013). Parcel-based change detection in land-use maps by adopting the holistic feature. IEEE Journal of Selected Topics in Applied Earth Observations and Remote Sensing, 7(8), 3482-3490.
11. Wang, K., Franklin, S. E., Guo, X., &Cattet, M. (2010). Remote sensing of ecology, biodiversity and conservation: A review from the perspective of remote sensing specialists. Sensors, 10(11), 9647-9667. https://doi.org/10.3390/s101109647
12. Semela, M., Ramoelo, A., &Adelabu, S. (2020). Testing and comparing the applicability of Sentinel-2 and Landsat 8 reflectance data in estimating mountainous herbaceous biomass

before and after fire using random forest modelling. In IGARSS 2020–2020 IEEE International Geoscience and Remote Sensing Symposium (pp. 4493–4496). IEEE. https://doi.org/10.1109/IGARSS39084.2020.9324048

13. Rahman, S., Chang, H.-C., Hehir, W., Magill, C., & Tomkins, K. (2018). Inter-comparison of fire severity indices from moderate (MODIS) and moderate-to-high spatial resolution (Landsat 8 & Sentinel-2A) satellite sensors. In IGARSS 2018–2018 IEEE International Geoscience and Remote Sensing Symposium (pp. 2873–2876). IEEE. https://doi.org/10.1109/IGARSS.2018.8518449
14. Izquierdo-Verdiguier, E., Moreno-Martínez, Á., Adsuara, J. E., Muñoz-Marí, J., Camps-Valls, G., Moneta, M. P., Kimball, J. S., Clinton, N., & Running, S. W. (2021). Global upscaling of the MODIS land cover with Google Earth Engine and Landsat data. In 2021 IEEE International Geoscience and Remote Sensing Symposium IGARSS (pp. 309-312). IEEE. https://doi.org/10.1109/IGARSS47720.2021.9554540
15. Young, N. E., Anderson, R. S., Chignell, S. M., Vorster, A. G., Lawrence, R., & Evangelista, P. H. (2017). A survival guide to Landsat preprocessing. Ecology, 98(4), 920-932.
16. Banskota, A., Kayastha, N., Falkowski, M. J., Wulder, M. A., Froese, R. E., & White, J. C. (2014). Forest monitoring using Landsat time series data: A review. Canadian Journal of Remote Sensing, 40(5), 362-384.
17. Hair, J. H., Reuter, D. C., Tonn, S. L., McCorkel, J., Simon, A. A., Djam, M., Alexander, D., Ballou, K., Barclay, R., Coulter, P., & others. (2018). Landsat 9 thermal infrared sensor 2 architecture and design. In IGARSS 2018-2018 IEEE International Geoscience and Remote Sensing Symposium (pp. 8841–8844). IEEE.
18. El Fellah, S., Rziza, M., & El Haziti, M. (2016). An efficient approach for filling gaps in Landsat 7 satellite images. IEEE Geoscience and Remote Sensing Letters, 14(1), 62–66.
19. Celik, N. (2018). Change detection of urban areas in Ankara through Google Earth Engine. In 2018 41st International Conference on Telecommunications and Signal Processing (TSP) (pp. 1-5). IEEE.
20. Miller, J. D., &Thode, A. E. (2007). Quantifying burn severity in a heterogeneous landscape with a relative version of the delta normalized burn ratio (dNBR). Remote Sensing of Environment, 109(1), 66-80.
21. Stehman, S. V. (1996). Estimating the kappa coefficient and its variance under stratified random sampling. Photogrammetric Engineering & Remote Sensing, 62(4), 401–407.
22. Pontius Jr, R. G., &Millones, M. (2011). Death to kappa: Birth of quantity disagreement and allocation disagreement for accuracy assessment. International Journal of Remote Sensing, 32(15), 4407-4429.
23. Stein, J., Aryal, J., &Gort, G. (2005). Generalized Bradley-Terry models and multi-class probability estimates. IEEE Transactions on Geoscience and Remote Sensing, 43(4), 852-856.
24. Walz, Y., Maier, S. W., Dech, S. W., Conrad, C., & Colditz, R. R. (2007). Classification of burn severity using moderate resolution imaging spectroradiometer (MODIS): A case study in the Jarrah-Marri forest of southwest Western Australia. Journal of Geophysical Research: Biogeosciences, 112(G2).
25. Epting, J., Verbyla, D., &Sorbel, B. (2005). Evaluation of remotely sensed indices for assessing burn severity in interior Alaska using Landsat TM and ETM+. Remote Sensing of Environment, 96(3-4), 328-339.
26. Ye, S., Pontius Jr, R. G., &Rakshit, R. (2018). A review of accuracy assessment for object-based image analysis: From per-pixel to per-polygon approaches. ISPRS Journal of Photogrammetry and Remote Sensing, 141, 137-147.
27. Jensen, J. R., et al. (1996). Introductory digital image processing: A remote sensing perspective (2nd ed.). Prentice-Hall Inc.
28. Uebersax, J. S. (1982). A generalized kappa coefficient. Educational and Psychological Measurement, 42(1), 181–183.
29. Henry, F., Herwindiati, D. E., Mulyono, S., &Hendryli, J. (2017). Sugarcane land classification with satellite imagery using logistic regression model. IOP Conference Series:

Materials Science and Engineering, 185(1), 012024.
30. Gholinejad, S., &Khesali, E. (2021). An automatic procedure for generating burn severity maps from the satellite images-derived spectral indices. International Journal of Digital Earth, 14(11), 1659-1673.
31. Laneve, G., Fusilli, L., Marzialetti, P., De Bonis, R., Bernini, G., &Tampellini, L. (2016). Development and validation of fire damage-severity indices in the framework of the PREFER project. IEEE Journal of Selected Topics in Applied Earth Observations and Remote Sensing, 9(6), 2806-2817.
32. Pakistan Bureau of Statistics. (2024). 7th Population and Housing Census 2023: Detailed Results. Retrieved from https://www.pbs.gov.pk/digital-census/detailed-results